High Temperature Superconducting Linear Motor Technology

JIN Jian-xun and ZHENG Lu-hai

(School of Automation Engineering, University of Electronic Science and Technology of China Chengdu 610054)

Abstract With the improvement of high temperature superconducting (HTS) material technology, HTS linear motors (LM) which are built using HTS bulks and HTS tapes have been realized. In this paper, different types of the developed HTS LMs are summarized with their structure models. The electromagnetic characteristics of these HTS LMs are studied with the results obtained by using magnetic field finite element method. Superiorities of the HTS LM technology are also verified with its applications in transportation field such as maglev and electromagnetic aircraft launcher.

Key words electromagnetic launchers; high temperature superconductors; linear motor; maglev vehicles; superconducting magnets

高温超导直线电动机技术

金建勋，郑陆海

(电子科技大学自动化工程学院 成都 610054)

【摘要】随着高温超导材料制备技术的进步，应用高温超导块材和带材研制开发直线电动机已具备了核心技术基础。该文总结了已研制出的高温超导直线电动机类型，并建立了它们的结构模型。应用磁场有限元方法，研究了这些不同类型高温超导直线电动机的电磁特性，并设计了实际模型装置进行了试验验证。通过高温超导直线电动机在磁悬浮车及电磁飞机弹射器等交通运输领域中的应用分析，验证了高温超导直线电动机技术在实际应用当中的潜在优越性。

关 键 词 电磁发射器； 高温超导体； 直线电动机； 磁悬浮运输装置； 超导磁体

中图分类号 TM37 **文献标识码** A doi:10.3969/j.issn.1001-0548.2009.05.013

The development of high temperature superconducting (HTS) materials has progressed more than twenty years, and the forms of HTS materials are mainly the HTS bulks, HTS tapes, and HTS films. In strong current application fields, HTS bulks and tapes have been commonly and widely applied into electric power, traffic, magnet etc. due to their excellent electromagnetic performance.

The HTS bulks with trapped magnetic field above 2.3 T in 77 K and 17 T in 29 K have been reported[1-2], which are substantially higher than conventional permanent magnet (PM). The applications of HTS bulk magnets into motors, flywheel energy storage devices and magnetic levitation systems have been initialized[3-5]. The secondary generation (2G) HTS tape, namely YBCO coated conductor, has well been developed after the first generation (1G) BSCCO/Ag tape manufacturing technologies being reaching maturity. Now, the critical current density of 1G HTS Bi-2223 tapes and 2G YBCO coated conductor have reached over 3×10^5 A/cm^2 (77 K, 0 T) and 3×10^6 A/cm^2 (77 K, 0 T), respectively[6-7].

With the performance progress of HTS bulks and HTS tapes, HTS linear motors (LM) using HTS materials have been developed with advanced characteristics and performances, which are suitable for a wide range of applications.

In this work, three different types of HTS LM theory models will be analyzed with their technologies presented in details. The time-step finite element

Received data: 2009 – 06 – 15
收稿日期：2009 – 06 – 15
Foundation item: Supported by the 863 Item under Grant No. 2007AA03Z208
基金项目：国家863计划(2007AA03Z208)
Biography: JIN Jan-xun was born in 1962, doctor, professor, Ph.D. adviser. His research interests mainly include applied superconductivity and energy efficiency technology.
作者简介：金建勋(1962 –)，男，博士，教授，博士生导师，主要从事高温超导应用技术及高效节能技术方面的研究.

method (FEM) is applied to solve these HTS LM models, and their electromagnetic characteristics are presented. The HTS LM application technologies used such as linear actuator and electromagnetic aircraft launcher are verified preliminarily with their application model built.

1 Model of HTS LSM

The linear motor mainly includes linear induction motor (LIM), permanent magnet linear synchronous motor (PMLSM) and linear reluctance motor (LRM). The HTS linear motors developed recently are mainly the linear synchronous motors (LSMs). Based on the different application models of HTS materials, the HTS LSMs are divided into the following types:

(1) HTS bulk magnet LSM with field-cooled (FC) HTS bulks magnet as secondary[8-11];

(2) HTS LSM with zero-field-cooled (ZFC) HTS bulk as secondary[12-13];

(3) HTS LSM with primary windings using HTS coils[14];

(4) Hybrid HTS LSM can be realized by combining (1) and (3) or (2) and (3).

Based on their structures, the HTS LSM can also be divided into single-sided primary LSM[10-11,14-15] and double-sided primary LSM[8-9,12-13]. The conventional LM integrated with HTS levitation systems is an important LM application with HTS technology, however it is only recognized as combined HTS LM applications here.

1.1 HTS LSM with FC HTS Bulk Magnets

A HTS bulk can trap magnetic field by FC magnetization with steady magnetic field or pulse magnetic field, as the schemes of a D.C. magnet and a pulse power supply are shown in Fig. 1. After being magnetized, the HTS bulk magnets are installed into the secondary of LSM with alternating poles of N and S in longitudinal direction, and same poles in transverse direction to achieve enough width. There are two types of motor structure with single-sided and double-sided developed as shown in Fig. 2a and Fig. 2b. For the single-sided HTS LSM, the back-iron may be used to improve the electromagnetic force. For the double-sided HTS-LSM, the magnetic attractive force between the primary iron-core and HTS bulk magnet secondary can be cancelled.

The sandpile model in combination with the Biot-Savart law can be used to build HTS bulk magnet numerical model[16], and the magnetic flux density $\boldsymbol{B}$ distribution of bulk magnet can be calculated based on it.

The fundamental wave electromagnetic thrust force F_{em} generated by HTS LSM is:

$$F_{em}=\frac{3p\pi N_c k_N I_1}{\sqrt{2}\tau}\psi_{SC} \tag{1}$$

where ψ_{SC} is the magnetic flux linkage one coil applied by one pole-pairs of HTS bulk magnets, N_c the turns of phase winding, k_N the winding factor, I_1 the phase current, τ the pole pitch, p the pole-pairs.

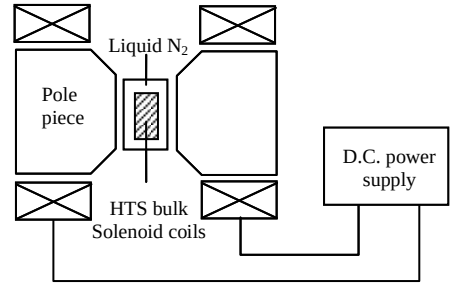

a. Static-field magnetization

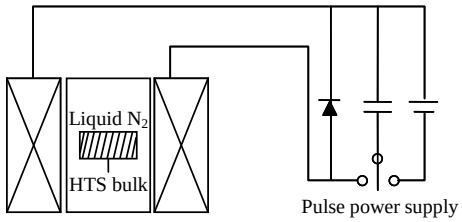

b. Pulse magnetization

Fig. 1 FC magnetizations

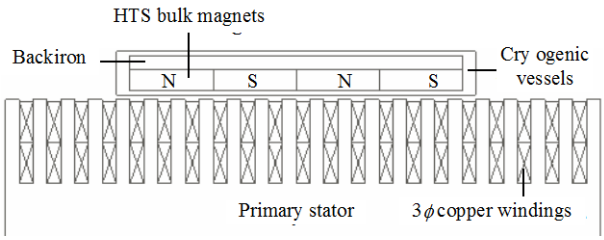

a. Single-sided HTS bulk magnet LSM

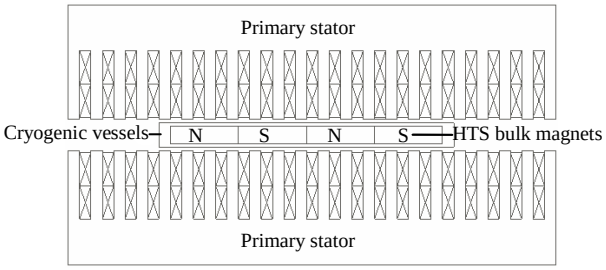

b. Double-sided HTS bulk magnet LSM

Fig. 2 HTS LSM with FC HTS bulk magnets

1.2 HTS LSM with ZFC HTS Bulks

A new type HTS LSM with ZFC HTS bulks is proposed based on the idea of position-holding characteristic of HTS bulk generating a synchronizing force with a travelling wave magnetic field generated by current-carrying armature winding.

The single-sided and double-sided HTS LSMs with ZFC HTS bulks as moving secondary have been studied and the physical structure models are shown in Fig. 3. The HTS bulks are cooled to superconducting state by liquid-N_2 in cryogenic vessels.

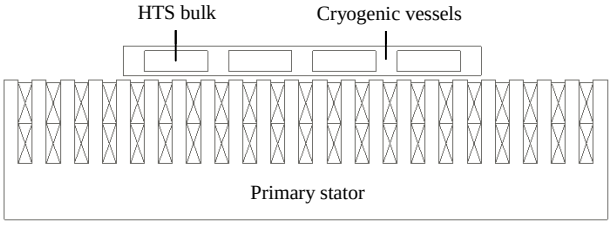

a. Single-sided HTS LSM

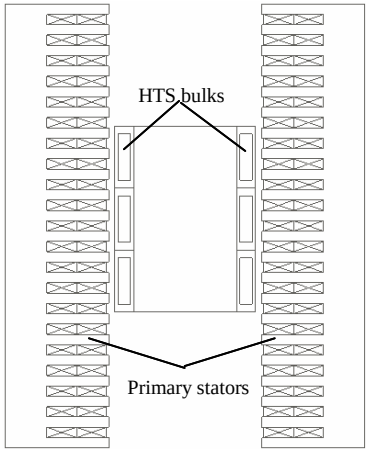

b. Double-sided HTS LSM

Fig. 3 HTS LSM with ZFC HTS bulks as secondary

Kim model can be used to analyze the electromagnetic characteristic of HTS bulk exposed to external magnetic field[17]. The current density J_c of HTS bulk varies with the external magnetic field and has the form

$$J_c(H_i,T)=\frac{J_c(T)}{1+H_i/H_0} \tag{2}$$

where $J_c(T)=J_{c0}(T_c-T)/(T_c-T_0)$, H_i the local magnetic field, T the temperature, H_0 the macroscopic materials parameter with the dimension of field, T_c the critical temperature, and J_{c0} the critical current density at the reference temperature T_0. The model was found to agree well with the experimental results when the sample was assumed to be a solid cylinder.

1.3 HTS LSM with HTS Coil Windings

The model of HTS LSM with HTS primary coils is shown in Fig. 4.

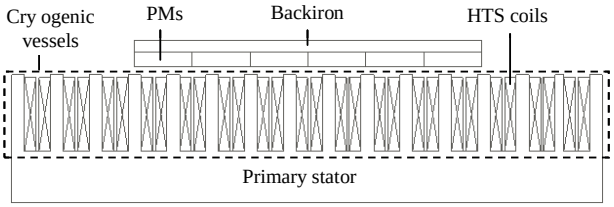

Fig. 4. HTS LSM with HTS coil windings

HTS pancake coils are used by wounding concentrated in one tooth for its easiness to manufacture. The conventional PMs and backiron are applied as secondary. The thrust force F_x and normal force F_y can be calculated simply from the *d*-*q* model equations. When the resistance of HTS coil windings R=0, the *d*-*q* model equations can be expressed as[18]

$$u_d=\frac{\mathrm{d}\psi_d}{\mathrm{d}t}-\omega\psi_q \tag{3}$$

$$u_q=\frac{\mathrm{d}\psi_q}{\mathrm{d}t}+\omega\psi_d \tag{4}$$

$$\psi_d=L_d i_d+M_{\mathrm{dp}}i_p,\ M_{\mathrm{dp}}=\sqrt{\frac{3}{2}}\frac{E_1}{\omega I_p} \tag{5}$$

$$\psi_q=L_q i_q,\ \ \psi_{\mathrm{PM}}=M_{\mathrm{dp}}i_p \tag{6}$$

where ψ_d and ψ_q are the flux linkage in the *d*-axis and *q*-axis respectively, ψ_{PM} the flux of the phase winding produced by the mover PMs; E_1 the back electromotive force (EMF), I_p the equivalent current of the PM corresponding to its coercive force and height, L_d and L_q the induction of *d*-axis and *q*-axis respectively, i_d and i_q the current of *d*-axis and *q*-axis respectively, M_{dp} the mutual inductance between the windings of *d*-axis and PMs. Based on the power balance procedure, we have:

$$F_x=\frac{P_e}{v}=\frac{\omega}{2\tau f}(\psi_d i_q-\psi_q i_d)=\frac{\pi}{\tau}(\psi_d i_q-\psi_q i_d)=\frac{\pi}{\tau}\left(\sqrt{\frac{3}{2}}\psi_{\mathrm{PM}}i_q+(L_d-L_q)i_d i_q\right) \tag{7}$$

$$F_y=i_d\frac{\partial\psi_d}{\partial g}+i_q\frac{\partial\psi_q}{\partial g} \tag{8}$$

where P_e is the electromagnetic power, v the linear velocity, ω the synchronous angular velocity, f the frequency, g the length of air-gap. When the LSM is the flat structure, we have L_d=L_q. For the P pairs poles

LSM, the thrust can be finally expressed as

$$F_x = p\sqrt{\frac{3}{2}}\frac{\pi}{\tau}\psi_{\mathrm{PM}} i_q \tag{9}$$

2 Electromagnetic Characteristics of HTS LSM

2.1 HTS LSM with FC HTS Bulk Magnets

The major dimensions and parameters of the simulation model of HTS LSM with FC HTS bulk magnets are shown in Table 1. The concentrated diametral winding is applied in the primary winding with the polar pitch of 45 mm. The relative permeability of HTS bulk magnet is assigned as μ=0.4 by experiences. The finite element model of HTS LSM is built as shown in Fig. 5 with the materials are numbered as:

① air, ② HTS bulk magnet North, ④ HTS bulk magnet South, ⑤ primary iron, ⑥ winding coils.

Table 1 Major dimensions of HTS bulk magnet HTS LSM

Primary	
Copper windings	
Number of turns	200
Diameter of copper wire/mm	1.18
Resistivity/Ω·m	1.75×10^{-8}
Iron core	
Tooth length (movement direction)/mm	10
Tooth width l_t/mm	150
Tooth depth/mm	100
Slot width/mm	20
Polar pitch τ	45
Main air gap g/mm	6
Secondary	
HTS bulk magnets	
Magnet length (movement direction) l_s/mm	45
Magnet width w_s/mm	50
Magnet height h_s/mm	12
Trapped magnetic field B/T	0.5
Relative permeability	0.4
Number of magnets along longitudinal direction	6
Number of magnets along transverse direction	3

The thrust F_x versus load angle characteristics are shown in Fig. 6 when the backiron is used or not. As can be seen from the graph, the thrust-angle curve is almost sinusoidal and has a peak at angle of 90° and 270°. It also indicates that the HTS LSM with backiron has bigger F_x than that without one. Fig. 7 shows the F_x versus the trapped field of HTS bulk for various air-gap length, and it shows that the F_x increases with the trapped field of HTS bulk, and decreases with the length of air-gap.

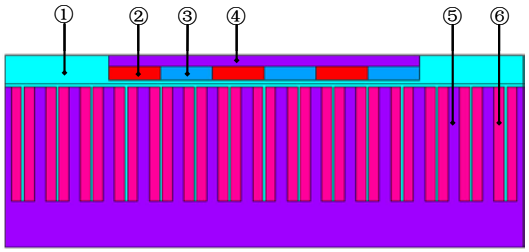

Fig. 5 Finite element model of HTS bulk magnet LSM

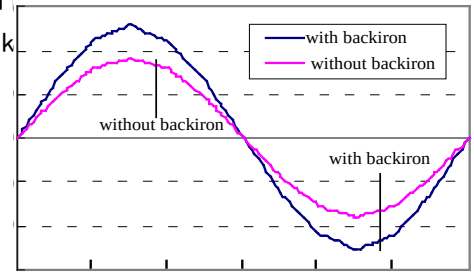

Fig. 6 F_x versus load angle characteristic with and without backiron.

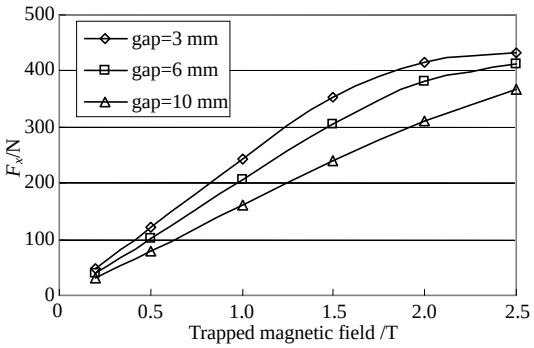

Fig. 7 F_x versus the trapped field of HTS bulk for various air-gap length

2.2 HTS LSM with ZFC HTS Bulks

The finite element model of the HTS LSM with ZFC HTS bulks is built based on the dimensions as shown in Table 1 without backiron and a small trapped magnetic field after the current is applied to the primary coils. Fig. 8 shows the thrust versus working current for various lengths of HTS bulk. It indicates that the thrust F_x increases with increasing of the current and the length of HTS bulks.

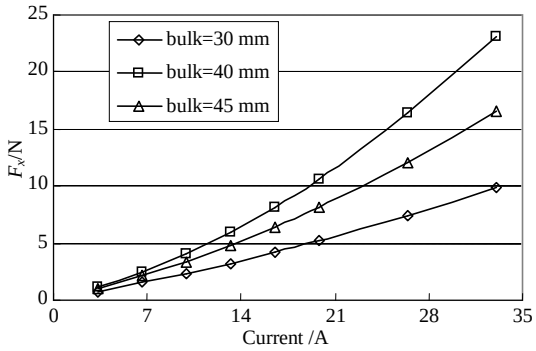

Fig. 8 F_x versus current for various lengths of HTS bulk

2.3 HTS LSM with HTS Coil Windings

Because of the zero-resistance characteristic of HTS tape, the larger current can be applied to the HTS coils. Fig. 9 shows the thrust F_x versus load angle characteristics for various working currents of HTS primary windings. As is indicated in the graph, the F_x can increase by 16.5 times to 2 840 N when the current changes from 3.3 A to 99 A, which can not be realized by conventional copper windings.

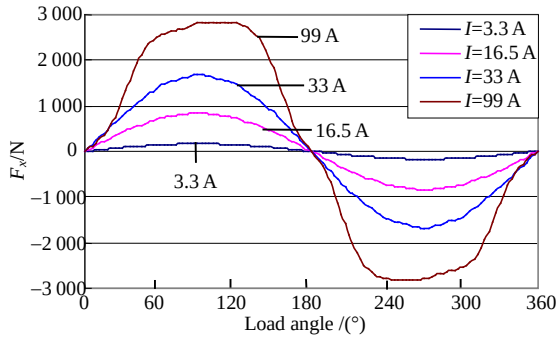

Fig. 9 F_x versus load angle for various currents of HTS coils

3 Application Technology of HTS LSM

3.1 HTS Magnetic Levitation Linear Actuator

The application model of HTS linear synchronous actuator is shown in Fig. 10, which is composed of a HTS LSM with HTS bulk magnets as moving secondary and HTS magnetic levitation systems on both sides of the HTS LSM. While the levitating force is directly proportional to the gradient of magnetic field over the PM-guideway, the lateral guidance force depends on the trapped flux in the HTS bulks. The HTS linear actuator can provide inherent stability in both vertical and lateral directions and realize self-levitation and self-guidance without any active control system.

The levitation force and guidance force are generated based on the pinning force or the shielding force of HTS bulks[19], and can be calculated by multiplying an external magnetic field by a shielding current flowing in a HTS bulk with the following equations:

$$F_{\mathrm{Lev}} = \int_0^{\mathrm{TH}} \int_{L/2}^{L/2-\delta} \int_{W/2}^{W/2-\delta} J_c B_x \mathrm{d}x\mathrm{d}y\mathrm{d}z \tag{10}$$

$$F_{\mathrm{Gui}} = \int_0^{\mathrm{TH}} \int_{L/2}^{L/2-\delta} \int_{W/2}^{W/2-\delta} J_c B_z \mathrm{d}x\mathrm{d}y\mathrm{d}z \tag{11}$$

where F_{Lev} is the levitation force, F_{Gui} the guidance force, J_c the critical current density, B_x the field along the transverse direction, B_z the field along the vertical direction, δ the depth of field penetration, L, W and TH are the length, width and thickness of a rectangle HTS bulk, respectively. In this paper, it is assumed that induced shielding currents flowing in the bulk body were equal to the critical currents. The δ used as integral range is given by the following relation:[20]

$$\delta = \frac{B_z - B_{\mathrm{zfc}}}{\lambda \mu_0 J_c} \tag{12}$$

where B_{zfc} is the trapped magnetic field, λ the Nagaoka coefficient determined by the configuration of a sample.

The HTS magnetic levitation linear actuator composed of HTS LSM and HTS magnetic levitation system with an optimal structure based on the construction as shown in Fig. 10 can be applied in transportation field such as maglev, industrial automation control and production transmission lines such as ropeless linear elevator, semiconductor manufacturing handling system, etc. Compared with the conventional linear motors, HTS LSMs have many obvious advantages such as smaller volume, bigger propulsion, and higher power factor in these applications.

Based on the theory analysis, a HTS LSM experimental device has been developed as shown in Fig. 11, which is composed of primary stator and secondary mover, and the secondary HTS bulk magnets are installed in a cryogenic vessel which is fixed on the secondary mover. Now, the mover can slide freely along the guide rails on both sides of the

stator, and the experimental slide rail will be replaced by the HTS levitation system.

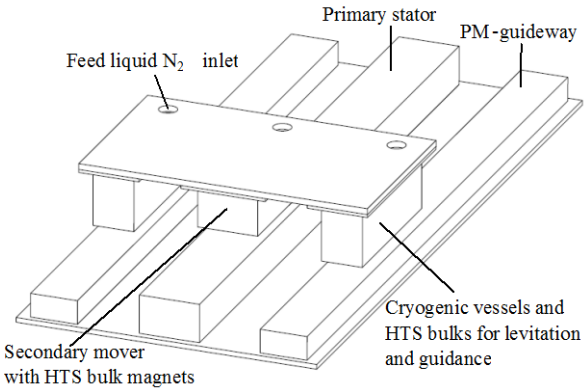

Fig. 10 A small scale prototype HTS bulk magnet LSM integrated with HTS levitation system.

Fig. 11 Experimental setup of the HTS LSM

3.2 Electromagnetic Aircraft Launcher

The realization of HTS bulk magnet HTS LSM for the electromagnetic aircraft launch system (EMALS) is shown in Fig. 12. The double-sided HTS LSM is integrated with a HTS magnetic levitation system, so that the slider and secondary rotor can move without any frication. The HTS bulk magnets are installed in a cryogenic vessels made by electrically and magnetically nonconductive material with the same pole in transverse direction and alternating poles of N and S in longitudinal direction as shown in Fig. 13. The specifications and technical features for the design of an EMALS include[9]: aircraft mass is 23 000 kg, maximum velocity is 103 m/s, maximal available path for acceleration is 94.49 m, maximal available path for deceleration is 5.79 m, acceleration, acceleration period are 56.01 m/s^2, 1.84 s, deceleration, deceleration period are 916.2 m/s^2, 0.112 s, goal energy is 122 MJ, goal thrust is 2 MN.

Based on the technical data presented above, the basic design dimensions and parameters for three types of linear motors containing LIM, PMLSM and HTS LSM are compared with the results shown in Table 2. It can be seen from Table 2 that an almost unity power factor can be obtained for the HTS bulk magnet LSM, which would result in a dramatic reduction in the size and cost of the power electronic converters. If the temperature can be reduced to around 40 K, a much smaller rotor mass can be obtained and such a HTS LSM could become the best candidate for this application in the future.

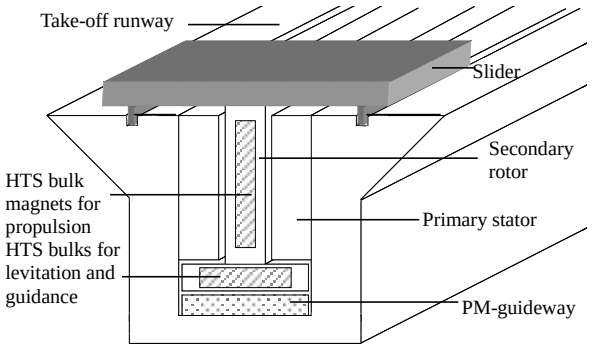

Fig. 12 HTS LSM integrated with HTS levitation system for electromagnetic aircraft launch

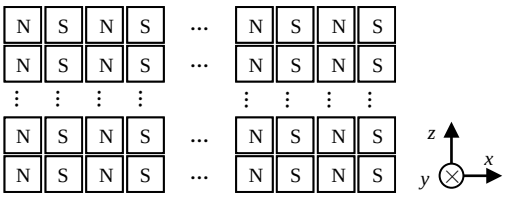

Fig. 13 Secondary HTS bulk magnet array

Table 2 Comparison of important data for LIM, PMLSM and HTS LSM[9]

	LIM	PMLSM	HTS LSM	
			77 K	Low T
Pole pitch	0.650	0.074	0.084	0.084
Rotor length in z/m	7.80	7.38	6.38	2.35
Rotor height in *y*/ m	3.96	2.13	2.14	2.14
Total rotor mass /kg	2 070	2 104	2 485	916
Inductance of stator coil/μH	0.840	1.215	0.052	0.052
Resistance of stator coil/μΩ	8.87	160.00	114.00	114.00
Frequency corresponding to 103 m/s	83	698	613	613
cosϕ (at speed 103 m/s)	0.106	0.642	0.999	0.999

4 Conclusions

The HTS LSM using either field-cooled or zero-field-cooled HTS bulk as secondary, and HTS coil windings as primary are proposed with their design model presented. The electromagnetic characteristics of these HTS LSMs have been studied using magnetic field FEM, with verification of the HTS LSM

prototype developed, and the analysis results on the models used show that: 1) the thrust can increase by 4.05 times when the trapped field of HTS bulk increases from 0.5 T to 2.5 T, 2) the thrust will increase by 16.5 times to 2 840 N when the coil current change from 3.3 A to 99 A for the LSM with HTS windings primary. The application models of HTS linear actuator and electromagnetic aircraft launcher are built with their characteristics presented, which have shown the superiorities of applying the HTS LSM technology in the transportation field.

References

[1] SAKAI N, KITA M, NARIKI S, et al. Field trapping property of Gd–Ba–Cu–O bulk superconductor 140 mm in diameter[J]. Physica C, 2006, 445-448: 339-342.

[2] TOMITA M, MURAKAMI M. High-temperature superconductor bulk magnets that can trap magnetic fields of over 17 tesla at 29 K[J]. Nature, 2003, 421(6922): 517-520.

[3] JIN J X, ZHENG L H, GUO Y G., et al. Development of high temperature superconducting machines[J]. J Jpn Soc Appl Electromagn Mech, 2007, 15(s): S88-S91.

[4] WANG S Y, WANG J S, WANG X Z, et al. The man-loading high temperature superconducting Maglev test vehicle[J]. IEEE Trans on Appl Super, 2003, 13(2): 1808-1811.

[5] STRASIK M, JOHNSON P E, DAY A C, et al. Design, fabrication, and test of a 5-kWh/100-kW flywheel energy storage utilizing a high-temperature superconducting nearing[J]. IEEE Trans on Appl Super, 2007, 17(2): 2133-2137.

[6] PATNAIK S, FELDMANN D M, POLYANSKII A A, et al. Local measurement of current density by magneto-optical current reconstruction in normally and overpressure processed Bi-2223 tapes[J]. IEEE Trans on Appl Super, 2003, 13(2): 2930-2933.

[7] SATHYAMURTHY S, PARANTHAMAN M, BHUIYAN M S, et al. Solution deposition approach to high Jc coated conductor fabrication[J]. IEEE Trans on Appl Super, 2005, 15(2): 2974-2976.

[8] SATO A, UEDA H, ISHIYAMA A. Operational characteristics of linear synchronous actuator with field-cooled HTS bulk secondary[J]. IEEE Trans on Appl Super, 2005, 15(2): 2234-2237.

[9] STUMBERGER G., AYDEMIR M T, THOMAS A L. Design of a linear bulk superconductor magnet synchronous motor for electromagnetic aircraft launch systems[J]. IEEE Trans on Appl Super, 2004, 14(1): 54-62.

[10] JIN J X, ZHENG L H. Performance analysis and optimization design of a HTS LSM[J]. J Sci, Technol Eng, 2008, 2(1): 19-22.

[11] JIN J X, ZHENG L H. Design and electromagnetic analysis of a HTS linear synchronous motor[C]//In Proc 2009 Int Conf Appl Super Electromag Devices. [S.l.]: [s.n.], 2009.

[12] TAKAHASHI A, UEDA H, ISHIYAMA A. Trial production and experiment of linear synchronous actuator with field-cooled hts bulk secondary[J]. IEEE Trans on Appl Super, 2003, 13(2): 2251-2254.

[13] YOSHIDA K, MATSUMOTO H. Propulsion and guidance simulation of a high-temperature superconducting bulk ropeless linear elevator[J]. IEEE Trans on Appl Super, 2004, 40(2): 615-618.

[14] MURAMATSU R, SADAKATA S, TSUDA M, et al. Trial production and experiments of linear actuator with HTS bulk secondary[J]. IEEE Trans on Appl Super, 2001, 11(1): 1976-1979.

[15] KIM W S, JUNG S Y, CHOI H Y, et al. Development of a superconducting linear synchronous motor[J]. IEEE Trans on Appl Super, 2002, 22(1): 842-845.

[16] FUKAI H, TOMITA M, MURAKAMI M, et al. Numerical simulation of trapped magnetic field for bulk superconductor[J]. Physica C, 2001, 357-360(SUPPL 2): 774-776.

[17] KIM Y B, HEMPSTEAD C F, STRNAD A R. Critical persistent currents in hard superconductors[J]. Phys Rev Lett, 1962, 9(7): 306-309.

[18] DENG Z, BOLDEA I, NASAR S. Forces and parameters of permanent magnet linear synchronous machines[J]. IEEE Trans on Magn, 1987, 23(1): 305-309.

[19] JIN J X. High Tc superconductor theoretical models and electromagnetic flux characteristics[J]. J Electron Sci Technol China, 2006, 4(3): 202-208.

[20] SUZUKI T, ARAKI S, KOIBUCHI K, et al. A study on levitation force and its time relaxation behavior for a bulk superconductor-magnet system[J]. Physica C, 2008, 468 (15-20): 1461-1464.

编 辑 漆 蓉

金建勋，博士，教授，博士生导师。1985年获北京钢铁学院(现北京科技大学)学士学位，1994年获澳大利亚新南威尔士大学硕士学位，1997年获澳大利亚卧龙岗大学博士学位。现研究方向主要包括高温超导应用技术及高效节能技术。

1991年起，在澳大利亚新南威尔士大学，开始从事高温超导应用研究，是澳大利亚最早从事高温超导强电应用及工业化发展研究的核心研究员，1992获得世界超导大会贡献奖。1997年成为澳大利亚研究理事会项目研究员，从事高温超导

强电及电力应用研究。2000年，作为澳大利亚高温超导应用研究的核心技术专家，成为澳大利亚研究理事会超导应用大型项目主要调研人，并负责澳大利亚超导公司高温超导工业化生产和测试，及高温超导电力应用技术和装置的研究和开发工作。

曾是最早在澳大利亚进行高温超导长线及磁体研究的人员，应用超导领域Wollongong(磁饱和)式高温超导限流器的首创者，高温超导高*Q*值电子电路共振理论和谐振器的发明人。主要研究工作包括高温超导电磁特性研究，高温超导测试技术，高温超导线圈与磁体技术研究；并研制了高温超导电力系统限流器、储能器、变压器、大电流引线、超导直流输电、电子高压发生器和高梯度场磁性分离器等实验模型装置。目前承担有国家863计划研究项目，研制开发结合高温超导磁悬浮系统的高温超导直线推进技术，并已取得了初步实用化的进展。

曾获得和完成多项政府、工业及大学研究项目；曾参与和完成多项与高温超导应用技术相关的技术发明，及开展多项创新技术研究和创新模型装置研制。已发表论文300余篇，两部应用超导专著和多项技术发明专利。受聘于多个国内国际学术组织，并参与了大量的各类学术活动。